

# Continuous Aperture Phased MIMO: Basic Theory and Applications

Akbar Sayeed  
Dept. of Electrical and  
Computer Engineering  
University of Wisconsin  
Madison, WI 53706  
Email: akbar@engr.wisc.edu

Nader Behdad  
Dept. of Electrical and  
Computer Engineering  
University of Wisconsin  
Madison, WI 53706  
Email: behdad@engr.wisc.edu

**Abstract**—Given the proliferation of wireless communication devices, the need for increased power and bandwidth efficiency in emerging technologies is getting ever more pronounced. Two technological trends offer new opportunities for addressing these challenges: mm-wave systems (60-100GHz) that afford large bandwidths, and multi-antenna (MIMO) transceivers that exploit the spatial dimension. In particular, there has been significant recent interest in mm-wave communication systems for high-rate (1-100 Gb/s) communication over line-of-sight (LoS) channels. Two competing designs dominate the state-of-the-art: i) traditional systems that employ continuous aperture “dish” antennas that offer high power efficiency but no spatial multiplexing gain, and ii) MIMO systems that use discrete antenna arrays to offer a higher multiplexing gain but suffer from power efficiency. In this paper, we propose a new communication architecture – continuous aperture phased MIMO – that combines the advantages of both designs and promises very significant capacity gains, and commensurate gains in power and bandwidth efficiency, compared to the state-of-the-art. CAP-MIMO is based on a hybrid analog-digital transceiver architecture that employs a novel antenna array structure – a high resolution discrete lens array – to enable a continuous-aperture phased-MIMO operation. We will present the basic theory behind CAP-MIMO and the potential capacity/power gains afforded by it. We will also highlight potential applications of CAP-MIMO in mm-wave communications.

## I. INTRODUCTION

The proliferation of data hungry wireless applications is driving the demand for higher power and bandwidth efficiency in emerging wireless transceivers. Two recent technological trends offer synergistic opportunities for meeting the increasing demands on wireless capacity: i) MIMO systems that exploit multi-antenna arrays for higher capacity by simultaneously multiplexing multiple data streams, and ii) millimeter-wave communication systems, operating in the 60-100GHz band that provide larger bandwidths. A key advantage of mm-wave systems, and very-high frequency systems in general, is that they offer high-dimensional MIMO operation with relatively compact array sizes. In particular, there has been significant recent interest in mm-wave communication systems for high-rate (1-100 Gb/s) communication over line-of-sight (LoS) channels. Two competing designs dominate the state-of-

the-art: i) traditional systems<sup>1</sup> that employ continuous aperture “dish” antennas and offer high power efficiency but no spatial multiplexing gain, and ii) MIMO systems that use discrete antenna arrays to offer a higher multiplexing gain but suffer from power efficiency; see, e.g., [1], [2], [3].

This paper develops the basic theory of a new MIMO transceiver architecture – continuous aperture phased (CAP) MIMO – that combines the elements of MIMO, continuous aperture antennas, and phased arrays for dramatically enhanced performance. CAP-MIMO is based on a *hybrid analog-digital transceiver architecture* that employs a novel antenna array structure – a *high resolution discrete lens array (DLA)* – to enable a *quasi continuous aperture* phased-MIMO operation. The DLA-based analog-digital interface also offers a low-complexity/low-cost alternative to *high-dimensional* phased arrays that employ digital beamforming for communication but are too complex and/or expensive to build at this time. In particular, in the context of gigabit LoS communication links, the CAP-MIMO system combines the attractive features of conventional state-of-the-art designs – the power gain of DISH systems and multiplexing gain of MIMO systems – to deliver very significant capacity gains and commensurate gains in power and bandwidth efficiency. Furthermore, the hybrid analog-digital architecture enables precise control of spatial beams for link optimization and point-to-multipoint network operation that is not possible with existing designs.

In a high-resolution DLA, a microwave lens with an appropriately designed *quasi-continuous phase profile* serves as the (continuous) radiating aperture that is excited by feed elements on an associated focal surface. Appropriately digitally processed data streams excite the feed elements on the focal surface whereas the signal propagation from the focal arc to the aperture of the DLA affects an analog spatial Fourier transform.

The basic mathematical framework for CAP-MIMO systems developed in this paper relies on a critically sampled discrete representation of continuous aperture antennas or radiating surfaces. The number of critical samples,  $n$ , represents the maxi-

<sup>1</sup>See, e.g., the commercial technology available from Bridgewave Communications; <http://www.bridgewave.com>

imum number of *analog spatial modes* that are excitable on the aperture. The resulting sampled system can be conceptualized in two complementary but equivalent ways: i) as an  $n \times n$  MIMO system with  $n$ -element antenna arrays at the transmitter and the receiver, or ii) as two coupled  $n$ -element phased uniform linear arrays (ULAs). In developing the basic CAP-MIMO theory, we leverage the connection between MIMO systems and phased ULAs from a communication perspective, that was first established in [4] and further developed in [5], [6].

The basic CAP-MIMO theory is applicable to a very broad class of communication links: short-range versus long-range, LoS versus multipath propagation, point-to-point versus network links. However, our focus is on high-frequency (mm-wave), high-rate (1-100 Gigabit/sec) LoS links, which could either be short-range (as in high-rate indoor applications, e.g. HDTV) or long-range (as in wireless backhaul). In such applications, out of the  $n$  possible analog modes, only  $p \ll n$  *digital modes* couple the transmitter and the receiver and can be used for simultaneously transmitting  $p$  data streams. The CAP-MIMO theory enables us to characterize the capacity (maximum reliable rate) for any such LoS link and the DLA-based analog-digital architecture enables us to approach the link capacity in practice with a significantly lower complexity compared to traditional phased arrays that employ digital beamforming.

In the next section, we present an overview of the CAP-MIMO system for LoS links with one-dimensional (1D) linear apertures and highlight its advantages over the two state-of-the-art competing designs : i) Conventional DISH systems that employ continuous aperture “dish” antennas, and ii) Conventional MIMO systems that use discrete multi-antenna arrays. The basic CAP-MIMO theory for 1D apertures is developed in Sections III-V, extension to 2D apertures is discussed in Sec. VI, representative numerical capacity comparisons are provided in Sec. VII, and details of the DLA-based realization of CAP-MIMO transceivers is discussed in Sec. VIII.

## II. OVERVIEW OF CAP-MIMO

Fig. 1 depicts a 1D LoS link in which the transmitter and receiver antennas have a linear aperture of length  $A$  and are separated by a distance  $R$ . Throughout, we assume that  $A \ll R$ . Let  $\lambda_c = c/f_c$  denote the wavelength of operation, where  $c$  is the speed of light and  $f_c$  is the carrier frequency. For  $f_c \in [60, 100]$ GHz,  $\lambda_c \in [3, 5]$ mm.

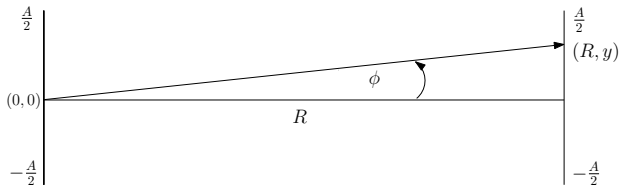


Fig. 1. The LoS channel.

For a given LoS link characterized by the physical parameters  $(A, R, \lambda_c)$ , as in Fig. 1, the CAP-MIMO framework

addresses the following fundamental question: **What is the link capacity at any operating signal-to-noise ratio (SNR)?** The CAP-MIMO theory is aimed at characterizing this fundamental limit and the DLA-based realization of the CAP-MIMO system is aimed at approaching this limit in practice. As elaborated in this paper, the two conventional designs, DISH and MIMO, are sub-optimum special cases of the CAP-MIMO framework.

The novel features of the CAP-MIMO transceiver architecture compared to state-of-art, include:

- The CAP-MIMO theory, that draws on insights, concepts and tools from MIMO communication theory, signal processing, and theory of phased arrays, enables us to accurately estimate the capacity of an inherently analog LoS link defined by continuous aperture antennas. (see Sec. II-D, Sec. IV and Sec. V).
- The CAP-MIMO system combines the attractive features of conventional state-of-the-art designs for LoS links – the power gain of DISH systems and multiplexing gain of MIMO systems – to deliver very significant capacity gains and commensurate gains in power and bandwidth efficiency. (see Sec. II-D, Sec. V and Sec. VII).
- The DLA-based realization of a CAP-MIMO system (see Sec. VIII) is based on new insights provided by the CAP-MIMO theory to approach the fundamental capacity of an LoS link in practice. In particular, the novel hybrid analog-digital architecture of a CAP-MIMO system enables high resolution analog beamforming and provides a significantly lower complexity analog-digital interface compared to traditional phased array-based architectures that employ digital beamforming (see Sec. II-C).
- The high resolution DLA-based hybrid analog-digital architecture enables precise control of spatial beams for robust operation in mobile scenarios and point-to-multipoint operation in network scenarios that is not possible with existing designs. (see Sec. II-E).
- While lens arrays have been used for directional signaling and beam steering, and provide an architecture for analog beamforming rather than digital beamforming in phased arrays [7], [8], [9], [10], [11], [12], [13], [14], capacity-approaching signaling and precise beam agility, afforded by the hybrid analog-digital CAP-MIMO architecture and enabled by a high-resolution DLA [15], is not possible with traditional lens arrays or high-resolution DLAs alone.

Sec. II-A introduces the concept of analog versus digital modes that play a key role in the CAP-MIMO framework. Sec. II-B introduces the DLA-based hybrid analog-digital architecture of a CAP-MIMO system for efficiently accessing the information carrying digital modes via *analog spatial beamforming*. Sec. II-C compares the complexity of the analog-digital interface of a DLA-based CAP-MIMO system to traditional approaches based on phased-arrays that use *digital beamforming*. Approximate closed-form expressions for capacity are presented in Sec. II-D. (The accuracy of the

closed-form expressions is assessed with exact capacity analysis in Sec. V.) Sec. II-E introduces the concept of beamwidth agility for realizing different configurations of a CAP-MIMO system that afford robustness in applications involving mobile links.

### A. Analog versus Digital Spatial Modes

To address the fundamental question of capacity, it is insightful to view the LoS link from two complementary but equivalent perspectives (see Sec. III): as a critically sampled MIMO system and as two coupled phased arrays [4], [5]. From a communication perspective, the continuous aperture antennas at the transmitter and the receiver can be equivalently represented by critically sampled (virtual)  $n$ -dimensional ULAs with antenna spacing  $d = \lambda_c/2$ , where  $n \approx 2A/\lambda_c$  is a fundamental quantity associated with a linear aperture antenna (electrical length). In other words, the analog spatial signals transmitted or received by the linear aperture antennas belong to an  $n$ -dimensional signal space. We term  $n$  as the *maximum number of independent analog (spatial) modes supported by the antennas*. These  $n$  spatial modes can, in turn be associated with  $n$  orthogonal spatial beams that cover the entire (one-sided) spatial horizon ( $-\pi/2 \leq \phi \leq \pi/2$  in Fig. 1) as illustrated in Fig. 2(a). However, due to the finite antenna aperture  $A$ , and large distance  $R \gg A$  between the transmitter and the receiver, only a small number of modes/beams,  $p_{max} \ll n$ , couple from the transmitter to the receiver, and vice versa, as illustrated in Fig. 2(b). We term  $p_{max}$  as the *maximum number of independent digital (spatial) modes supported by the LoS link*. The number of digital

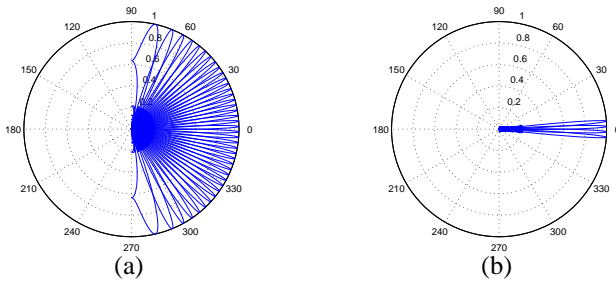


Fig. 2. CAP-MIMO beam patterns:  $n = 40$ ,  $p_{max} = 4$ . (a) The  $n = 40$  orthogonal beams covering the entire spatial horizon. (b) The  $p_{max} = 4$  orthogonal beams that couple the finite-aperture transmitter and receiver antennas.

modes,  $p_{max}$ , is a fundamental quantity related to the LoS link and can be calculated as  $p_{max} \approx A^2/(R\lambda_c)$  (see (21)). The  $p_{max}$  digital modes supported by the LoS link carry the information bearing signals from the transmitter to the receiver and govern the link capacity. In other words, the information bearing signals in the LoS link lie in a  $p_{max}$ -dimensional subspace of the  $n$ -dimensional spatial signal space associated with the antennas.

### B. DLA-based Hybrid Analog-Digital Architecture

Fig. 3 shows a (baseband) schematic of a DLA-based hybrid analog-digital architecture for realizing a CAP-MIMO

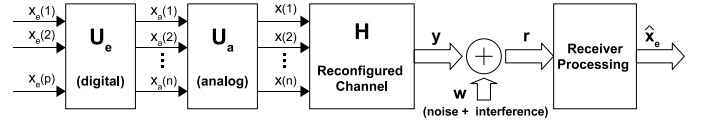


Fig. 3. The hybrid analog-digital architecture of a CAP-MIMO system. The analog operation of the DLA is represented by the transform  $U_a$ .

system. At the transmitter the architecture enables direct access to the  $p$  digital modes,  $1 \leq p \leq p_{max}$ , denoted by the input signals  $x_e(i)$ ,  $i = 1, \dots, p$ . A variety of well-known approaches, collectively called space-time coding techniques, can be used for encoding information into the  $p$  digital inputs  $\{x_e(i)\}$ . In the simplest case - spatial multiplexing [16] -  $x_e(i)$ ,  $i = 1, \dots, p$  represent  $p$  independent digital data streams. These independent digital signals are then mapped into  $n$  feed signals,  $x_a(i)$ ,  $i = 1, \dots, n$ , on the focal surface of the DLA, via the digital transform  $U_e$ . While not shown, the D/A conversion, including up-conversion to the passband at  $f_c$  is done at the output of  $U_e$ . (As noted next, the complexity of this D/A interface is on the order of  $p_{max} \ll n$ , rather than  $n$  in a conventional phased-array-based implementation.) The analog (up converted) signals on the focal surface of the DLA excite the  $n$  analog spatial modes on the continuous radiating aperture of the DLA, via the analog transform  $U_a$ . The analog signals on the DLA aperture are represented by their critically sampled version  $x(i)$ ,  $i = 1, \dots, n$  in Fig. 3.

We focus on the transmitter structure – the receiver also uses a DLA-based architecture to map the analog spatial signals on the DLA aperture to signals in beamspace via  $n$  sensors appropriately placed on the the focal surface. A subset of  $n$  signals on the focal surface of the receiver DLA is then down-converted and converted into baseband digital signals via an A/D. (The complexity of this A/D interface, as in the case of the transmitter, is again on the order of  $p_{max} \ll n$ , rather than  $n$  as in a conventional phased-array-based design using digital beamforming.) The digital signals are then appropriately processed, using any of a variety of well-known algorithms (e.g. maximum likelihood) to recover an estimate,  $\hat{x}_e(i)$ ,  $i = 1, \dots, p$ , of the transmitted digital signals. The nature of decoding/estimation algorithms at the receiver is dictated by the nature of digital encoding at the transmitter.

The transmitter is represented by two transforms: the digital transform  $U_e$  maps  $p$  digital symbols (corresponding to  $p$  data streams) to  $n$  analog symbols that excite  $n$  feeds on the focal arc of the DLA. The number of data streams  $p$  can be anywhere in the range from 1 to  $p_{max}$ .

The analog transform  $U_a$  represents the *analog spatial transform* between the focal surface and the continuous radiating aperture of the DLA. This continuous Fourier transform is affected by the wave propagation between the focal surface and the aperture of the DLA. However, consistent with the critical sampling of the aperture outlined in Sec. II-A, this continuous Fourier transform can be accurately approximately

by an  $n \times n$  discrete Fourier transform (DFT) matrix  $\mathbf{U}_a$  (see (15)) corresponding to critical sampling of the aperture and the focal arc (surface in 2D).

The  $n \times p$  digital transform matrix  $\mathbf{U}_e$  represents mapping of the  $p$ ,  $1 \leq p \leq p_{max}$ , independent digital signals onto the focal surface of the DLA, which is represented by  $n$  samples. Different values of  $p$  represent the different CAP-MIMO configurations (See Sec. II-D and Sec. II-E). For  $p = p_{max}$ , the digital component is the identity transform. For  $p < p_{max}$ , the digital transform effectively maps the digital signals to the focal arc so that  $p$  data streams are mapped onto  $p$  beams with wider beamwidths. Wider beamwidths, in turn, are attained via excitation of part of the aperture. (see Sec. VIII).

### C. Analog-Digital Interface Complexity: CAP-MIMO versus Phased Arrays

The DLA-based CAP-MIMO transceiver architecture provides the lowest-complexity analog-digital interface for accessing the  $p_{max}$  digital modes in a LoS link. To see this, it is instructive to compare the CAP-MIMO transmitter with a comparable transmitter based on an  $n$ -element phased array.

To think in terms of a phased array, imagine that the continuous transmitter aperture in Fig. 1 is replaced with an  $n$ -element phased array, where each element is associated with its own RF chain, including an D/A converter and an up-converter. In a phased-array, the  $p_{max}$  digital modes can be accessed via *digital beamforming* - each digital symbol, corresponding to a particular digital mode/beam is associated with an  $n$ -dimensional phase profile across the entire  $n$ -element phased array (the phase profile corresponds to a particular column of the  $n \times n$  DFT matrix  $\mathbf{U}_a$  (see (15)). As a result, while only a small number  $p_{max} \ll n$  of digital symbols are simultaneously transmitted (spatial multiplexing), all  $n$  elements of the phased array are involved in encoding the symbol into a corresponding spatial beam via digital beamforming. Thus, the D/A interface of a phased array-based system is  $n$ -dimensional or has complexity  $n$  -  $n$  independent RF chains, each with its own D/A and up-converter, are needed.

In a DLA-based CAP-MIMO transmitter, the  $p_{max}$  digital modes are accessed via *analog beamforming*: each digital symbol (represented by an output of the digital transform  $\mathbf{U}_e$ ), corresponding to a particular digital mode/beam, is associated with a corresponding feed-element on the focal surface of the DLA. Thus, even though the digital transform  $\mathbf{U}_a$  is  $n \times p$  for general operation, only on the order of  $p_{max} \ll n$  outputs are non-zero or active and as a result a corresponding number of feed elements (represented by  $\{x_a(i)\}$  in Fig. 3) are active on the focal surface of the DLA. As mentioned above, the D/A interface in a CAP-MIMO system is between the output of the digital transform  $\mathbf{U}_e$  and the input of the analog transform  $\mathbf{U}_a$ . Thus, the the D/A interface in a DLA-based CAP-MIMO system has a complexity on the order of  $p_{max}$ , rather than the order  $n$  complexity in a phased-array - only on the order or  $p_{max} \ll n$  independent RF chains, each with its on D/A an up-converter, are needed. When  $p = p_{max}$ , corresponding

to the multiplexing (MUX) configuration of the CAP-MIMO system, the D/A complexity is exactly  $p_{max}$ . When  $p < p_{max}$ , the complexity is a little higher than  $p_{max}$  (to realize robust beams with wider beamwidths), but still much smaller than  $n$ . (see Sec. VIII)

### D. Capacity Comparison

In this section, we present idealized closed-form expressions that provide accurate approximations for the capacity of the CAP-MIMO system and the two competing state-of-the-art designs, DISH and MIMO systems, for a 1D LoS link depicted in Fig. 1. The rationale behind these closed-form approximations is presented in Sec. IV.

1) *Conventional MIMO System*: Our starting point is the conventional MIMO system that uses a ULA with  $p_{max}$  antennas -  $p_{max}$  also reflects the maximum multiplexing gain or the maximum number of *digital modes* supported by the system. The required antenna spacing (Rayleigh spacing) to create  $p_{max}$  orthogonal spatial modes between the transmitter and the receiver is given by

$$d_{ray} = \sqrt{\frac{R\lambda_c}{p_{max}}} \quad (1)$$

and the corresponding aperture is given by

$$A = p_{max}d_{ray} \quad (2)$$

Ignoring path loss, and assuming omnidirectional antennas, the capacity of the conventional MIMO system is given by

$$C_{mimo} = p_{max} \log(1 + \rho\sigma_c^2/p_{max}^2) = p_{max} \log(1 + \rho) \quad (3)$$

where  $\rho$  denotes the total transmit SNR (signal-to-noise ratio) and  $\sigma_c^2 = p_{max}^2$  is the total channel power (captured by  $p_{max}^2$  transmit and receive omnidirectional antenna pairs). If higher gain antennas are used, the capacity expression (3) can be modified by replacing with a higher effective  $\rho$  reflecting the antenna gains.

2) *Conventional DISH System*: For a given aperture,  $A$ , defined in (2), the maximum number of *analog modes*,  $n$ , is the number of Nyquist samples, spaced by  $d = \lambda_c/2$ , that we can pack within the aperture

$$A = nd = n \frac{\lambda_c}{2} \iff n = \frac{2A}{\lambda_c}. \quad (4)$$

In practice,  $n$  can be taken as  $\lfloor n \rfloor$ . For the purposes of our comparison, we will approximate the continuous aperture DISH system with a corresponding MIMO system equipped with an  $n$ -element ULA at critical spacing  $d = \lambda_c/2$ . The DISH system has a higher total channel power  $\sigma_c^2 = n^2$  due to the continuous aperture which, in an ideal setting, is equally distributed between the  $p_{max}$  digital modes supported by the LoS link. Thus, since the DISH system transmits a single data stream compared with  $p_{max}$  streams in the MIMO system, the capacity of the DISH system can be accurately approximated as

$$C_{dish} \approx \log\left(1 + \frac{\rho\sigma_c^2}{p_{max}}\right) = \log\left(1 + \frac{\rho n^2}{p_{max}}\right) \quad (5)$$

3) *CAP-MIMO System*: The CAP-MIMO system combines the attractive features of DISH (high channel power - antenna gain) with those of MIMO (multiplexing gain). Furthermore, CAP-MIMO system has the agility to adapt the number of data streams,  $p$ ,  $1 \leq p \leq p_{max}$ . The capacity of the CAP-MIMO system for any  $p \in \{1, 2, \dots, p_{max}\}$  can be accurately approximated as

$$C_{c-mimo}(p) \approx p \log \left( 1 + \frac{\rho \sigma_c^2}{pp_{max}} \right) = p \log \left( 1 + \frac{\rho n^2}{pp_{max}} \right) \quad (6)$$

where  $\sigma_c^2 = n^2$  as in the DISH system. We focus on three CAP-MIMO configurations:

- **Multiplexing (MUX) configuration** -  $p = p_{max}$  - that yields the highest capacity.
- **Intermediate (INT) configuration** -  $p = \sqrt{p_{max}}$  - that yields medium capacity.
- **Beamforming (BF) configuration** -  $p = 1$  - that yields the lowest capacity, equal to that of the DISH system.

Fig. 4 shows the capacities of different systems along with the three CAP-MIMO configurations. The BF configuration coincides with the DISH configuration. The figure corresponds to a linear array with aperture  $A = .43\text{m}$ , link length of  $R = 2.75\text{m}$ , operating at  $f_c = 10\text{ GHz}$  with  $p_{max} = 4$  and  $n = 29$ . As evident from the figure, between the two conventional systems, MIMO dominates at high SNRs whereas DISH dominates at low SNRs. CAP-MIMO on the other hand, exceeds the performance of both conventional systems over the entire SNR range.

Fig. 5 compares DISH, MIMO and CAP-MIMO MUX configuration for a 60GHz link with  $A_p = 3.35\text{m}$ ,  $R = 1\text{km}$ ,  $p_{max} = 4$  and  $n = 1342$ . The performance gains of CAP-MIMO over DISH and MIMO are even more pronounced in this case.

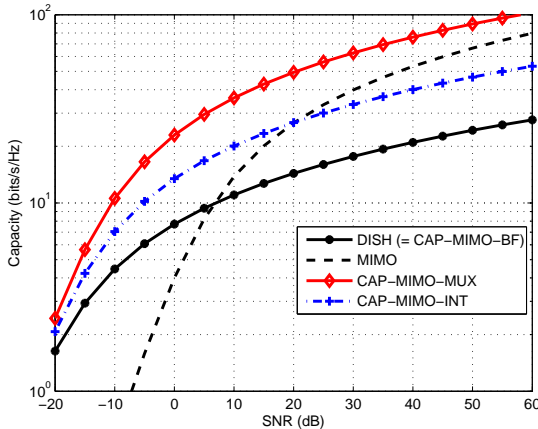


Fig. 4. Capacity comparison at 10 GHz

### E. CAP-MIMO Configurations: Beam Agility

As noted above, for a given  $p_{max}$ , the CAP-MIMO system can achieve a multiplexing gain of  $p$  where  $p$  can take on any

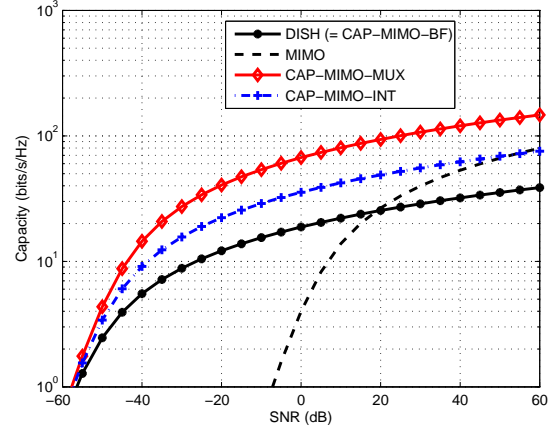


Fig. 5. Capacity comparison at 60 GHz

value between 1 and  $p_{max}$  corresponding to different CAP-MIMO configurations. The number of spatial beams used for communication is equal to  $p$ . While the highest capacity is achieved for  $p_{max}$ , lower values of  $p$  are advantageous in applications involving mobile links in which the transmitter and/or the receiver are moving. This is because of the beam agility capacity of the CAP-MIMO system: for  $p < p_{max}$ , by appropriately reconfiguring the digital transform  $\mathbf{U}_e$ , the  $p$  data streams can be encoded into  $p$  beams with *wider beamwidths* which still cover the entire aperture of the receiver array. The use of wider beamwidths relaxes the channel estimation requirements in the CAP-MIMO system.

Fig. 6 illustrates the notion of beam agility for a system using linear apertures with  $n = 40$  and  $p_{max} = 4$ . Fig. 6(a) shows the beampatterns for the MUX configuration for which  $p = p_{max} = 4$  - 4 narrow beams couple with the receiver aperture. Fig. 6(b) shows the beampatterns for an INT configuration with  $p = 2$ . In this case 2 beams are used for simultaneously transmitting 2 independent data streams but the beamwidth is twice the beamwidth in the MUX configuration. As a result the 2 beams still cover the entire receiver aperture. Fig. 6(c) shows the beampatterns for the BF configuration with  $p = 1$ . In this case a single data stream is encoded into a single beam with the largest beamwidth - 4 times the beamwidth in the MUX configuration. The BF configuration can be thought of as the CAP-MIMO configuration that represents an optimized conventional DISH system - the capacity of a conventional DISH system cannot exceed the capacity of the BF configuration in a CAP-MIMO system. We note that for  $p < p_{max}$  wider beamwidths are achieved via reconfigured versions of the digital transform  $\mathbf{U}_e$  that correspond to illuminating a smaller fraction of the DLA aperture. This, in turn, requires excitation of a few more than  $p_{max}$  elements on the focal surface of the DLA thereby slightly increasing the A/D complexity of the CAP-MIMO system (see Sec. VIII for details).

Fig. 7 illustrates the point-to-multipoint capability of a

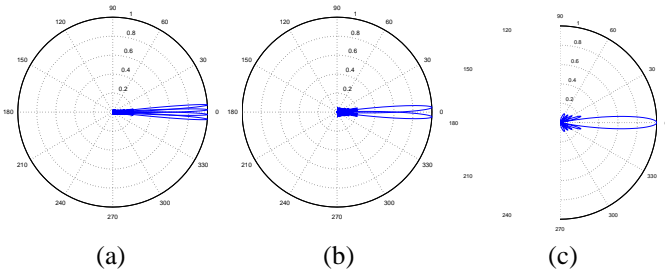


Fig. 6. CAP-MIMO Beampatterns for the three configurations for  $n = 40$  and  $p_{max} = 4$ . (a) MUX  $p = 4$ . (b) INT  $p = 2$ , (c) BF  $p = 1$ .

CAP-MIMO system in which a single CAP-MIMO transmitter simultaneously transmits to  $K = 4$  spatially distributed receivers in a network setting. In the illustration  $n = 40$  and  $p_{max} = 4$  for each individual link. Thus,  $p_{max} = 4$  data streams are simultaneously transmitted to each receiver, via the corresponding beams, resulting in a total of  $p_{max}K = 16$  streams/beams. We note that in practice  $n \gg p_{max}$  and as a result for relatively small values of  $K$ ,  $p_{max}K \ll n$  and the complexity of the D/A interface is still much smaller than a traditional phased-array based system.

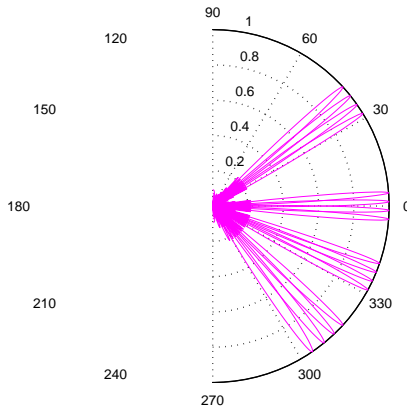


Fig. 7. CAP-MIMO beampatterns for enabling point-to-multipoint operation in the MUX configuration;  $n = 40$  and  $p_{max} = 4$ .

### III. SYSTEM MODEL

In this section, we develop a common framework for developing the basic theory of CAP-MIMO and comparing it with the two conventional designs: continuous-aperture DISH designs, and conventional MIMO designs. Our emphasis is on mm-wave systems in LoS channels. We first develop our framework for one-dimensional (1D) linear arrays and then comment on two-dimensional (2D) arrays in Sec. VI. It is insightful to view the LoS link in Fig. 1 from two perspectives: as a sampled MIMO system and as two coupled phased arrays. This connection between MIMO systems and phased arrays was first established in [4].

#### A. The LoS Channel: MIMO meets Phased Arrays

Fig. 1 depicts the LoS channel in the 1D setting. The transmitter and receiver consist of a continuous linear aperture of length  $A$  and are separated by a distance  $R \gg A$ . The center of the receiver array serves as the coordinate reference: the receiver array is described by the set of points  $\{(x, y) : x = 0, -A/2 \leq y \leq A/2\}$  and the transmitter array is described by  $\{(x, y) : x = R, -A/2 \leq y \leq A/2\}$ . While the LoS link can be analyzed using a continuous representation [5], in this paper we focus on a critically sampled system description, with spacing  $d = \lambda_c/2$ , that results in no loss of information and provides a convenient finite-dimensional system description for developing our framework [4].

For a given sample spacing  $d$ , the point-to-point communication link in Fig. 1 can be described by an  $n \times n$  MIMO system

$$\mathbf{r} = \mathbf{H}\mathbf{x} + \mathbf{w} \quad (7)$$

where  $\mathbf{x} \in \mathcal{C}^n$  is the transmitted signal,  $\mathbf{r} \in \mathcal{C}^n$  is the received signal,  $\mathbf{w} \sim \mathcal{CN}(\mathbf{0}, \mathbf{I})$  is the AWGN noise vector,  $\mathbf{H}$  is the  $n \times n$  channel matrix, and the dimension of the system is given by

$$n = \left\lfloor \frac{A}{d} \right\rfloor. \quad (8)$$

For critical spacing  $d = \lambda_c/2$ ,  $n \approx 2A/\lambda_c$  which represents the maximum number of independent spatial (analog) modes excitable on the array apertures.

The fundamental performance limits of the LoS link are governed by (the eigenvalues of) the channel matrix  $\mathbf{H}$ . In this paper, we will consider beamspace representation of  $\mathbf{H}$  [4]. Furthermore, we will be dealing with discrete representations of signals both in the spatial and beamspace domains. We use the following convention for the set of (symmetric) indices for describing a discrete signal of length  $n$

$$\mathcal{I}(n) = \{i - (n - 1)/2 : i = 0, \dots, n - 1\} \quad (9)$$

which corresponds to an integer sequence passing through 0 for  $n$  odd and non-integer sequence that does not pass through 0 when  $n$  is even. It is convenient to use the *spatial frequency* (or normalized angle)  $\theta$  that is related to the physical angle  $\phi$  as [4]

$$\theta = \frac{d}{\lambda_c} \sin(\phi). \quad (10)$$

The beamspace channel representation is based on  $n$ -dimensional array response/steering (column) vectors,  $\mathbf{a}_n(\theta)$ , that represent a plane wave associated with a point source in the direction  $\theta$ . The elements of  $\mathbf{a}_n(\theta)$  are given by

$$a_{n,i}(\theta) = e^{-j2\pi\theta i}, \quad i \in \mathcal{I}(n) \quad (11)$$

$$(12)$$

Note that  $\mathbf{a}(\theta)$  are periodic in  $\theta$  with period 1 and

$$\begin{aligned} \mathbf{a}_n^H(\theta')\mathbf{a}_n(\theta) &= \sum_{i \in \mathcal{I}(n)} a_{n,i}(\theta)a_{n,i}^*(\theta') = \sum_{i \in \mathcal{I}(n)} e^{-j2\pi(\theta - \theta')i} \\ &= \frac{\sin(\pi n(\theta - \theta'))}{\sin(\pi(\theta - \theta'))} \triangleq f_n(\theta - \theta') \end{aligned} \quad (13)$$

where  $f_n(\theta)$  is the Dirichlet sinc function, with a maximum of  $n$  at  $\theta = 0$ , and zeros at multiples of  $\Delta\theta_o$  where

$$\Delta\theta_o = \frac{1}{n} \approx \frac{d}{A} \iff \Delta\phi_o \approx \frac{\lambda_c}{d} \Delta\theta_o = \frac{\lambda_c}{A} \quad (14)$$

which is a measure of the *spatial resolution* or the *width of a beam* associated with an  $n$ -element phased array.

The  $n$ -dimensional signal spaces, associated with the transmitter and receiver arrays in an  $n \times n$  MIMO system, can be described in terms of the  $n$  orthogonal spatial beams represented by appropriately chosen steering/response vectors  $\mathbf{a}_n(\theta)$  defined in (12). For an  $n$ -element ULA, with  $n = A/d$ , an orthogonal basis for the  $\mathcal{C}^n$  can be generated by uniformly sampling the principal period  $\theta \in [-1/2, 1/2]$  with spacing  $\Delta\theta_o$  [4]. That is,

$$\mathbf{U}_n = \frac{1}{\sqrt{n}} [\mathbf{a}_n(\theta_i)]_{i \in \mathcal{I}(n)} \quad , \quad \theta_i = i\Delta\theta_o = \frac{i}{n} = i\frac{d}{A} \quad (15)$$

is an orthogonal (DFT) matrix with  $\mathbf{U}_n^H \mathbf{U}_n = \mathbf{U}_n \mathbf{U}_n^H = \mathbf{I}$ . For critical spacing,  $d = \lambda_c/2$ , the orthogonal beams corresponding to the columns of  $\mathbf{U}_n$ , cover the entire range for physical angles  $\phi \in [-\pi/2, \pi/2]$ .

For developing the beamspace channel representation, we need to relate the beam direction  $\theta$  at the receiver to points on the transmitter aperture. As illustrated in Fig. 1, a point  $y$  on the transmitter array represents a plane wave impinging on the receiver array from the direction  $\phi \approx \sin(\phi)$  with the corresponding  $\theta$  given by (10)

$$\sin(\phi) = \frac{y}{\sqrt{R^2 + y^2}} \approx \frac{y}{R} \iff \theta = \frac{dy}{\lambda_c R} \quad (16)$$

Using (16), we note the following correspondence between the sampled points on the transmitter array and the corresponding angles subtended at the receiver array

$$y_i = id \iff \theta_i = i\frac{d^2}{R\lambda_c} \quad , \quad i \in \mathcal{I}(n) \quad (17)$$

which for critical sampling  $d = \lambda_c/2$  reduces to

$$y_i = i\frac{\lambda_c}{2} \iff \theta_i = i\frac{\lambda_c}{4R} \quad , \quad i \in \mathcal{I}(n). \quad (18)$$

Finally, the  $n$  columns of matrix  $\mathbf{H}$  are given by  $\mathbf{a}(\theta)$  corresponding to the  $\theta_i$  in (18); that is,

$$\mathbf{H} = [\mathbf{a}_n(\theta_i)]_{i \in \mathcal{I}(n)} \quad , \quad \theta_i = i\Delta\theta_{ch} = i\frac{\lambda_c}{4R}. \quad (19)$$

We define the total channel power as

$$\sigma_c^2 = \text{tr}(\mathbf{H}^H \mathbf{H}) = n^2. \quad (20)$$

### B. Channel Rank: Coupled Orthogonal Beams

For the LoS link in Fig. 1, the link capacity is directly related to the rank of  $\mathbf{H}$  which is in turn related to the number of orthogonal beams from the transmitter that lie within the aperture of the receiver array, which we will refer to as the *maximum number of digital modes*,  $p_{max}$ . Fig. 2(a) shows the far-field beampatterns corresponding to the  $n$  orthogonal beams defined in (15) for  $n = 40$  that cover the entire spatial

horizon. Of these beams, only  $p_{max} = 4$  couple to the receiver array with a limited aperture, as illustrated in Fig. 2(b). The number  $p_{max}$  can be calculated as

$$p_{max} = \frac{2\theta_{max}}{\Delta\theta_o} = 2\theta_{max}n = 2\theta_{max}\frac{A}{d} \approx \frac{A^2}{R\lambda_c} \quad (21)$$

where  $\theta_{max}$  denotes the (*normalized*) *angular spread* subtended by the receiver array at the transmitter; we have used (10) and (16), noting that  $\sin(\phi_{max}) \approx \frac{A}{2R}$ , where  $\phi_{max}$  denotes the physical (one-sided) angular spread subtended by the receiver array at the transmitter.

We note that  $p_{max}$  in (21) is a fundamental link quantity that is independent of the antenna spacing used. For the conventional DISH system and the CAP-MIMO system we use  $d = \lambda_c/2$ . A conventional MIMO system, on the other hand, uses  $p_{max}$  antennas with spacing  $d_{ray}$ ; plugging  $A = p_{max}d$  in (21) leads to the required (Rayleigh) spacing  $d_{ray}$  in (1). The maximum number of digital modes,  $p_{max}$ , defined in (21) is a baseline indicator of the rank of the channel matrix  $\mathbf{H}$ . The actual rank depends on the number of dominant eigenvalues of  $\mathbf{H}^H \mathbf{H}$  as discussed in Sec. V.

### C. CAP-MIMO versus MIMO Beampatterns: Grating Lobes

Fig. 8 illustrates a key difference in the beampatterns of a CAP-MIMO system and conventional MIMO system. Fig. 8(a) illustrates two of the  $p_{max} = 4$  orthogonal beams that couple with the receiver in a CAP-MIMO system with  $n = 40$ . Fig. 8(b) illustrates the same two beams corresponding to a MIMO system with  $p_{max}$  antennas with spacing  $d_{ray}$ . As evident, each beam exhibits  $n_g = n/p_{max} = 10$  peaks – one of which lies within the receiver aperture while the remaining 9 (grating lobes) do not couple to the receiver.<sup>2</sup> These grating lobes result in overall channel power loss proportional to  $n_g^2$  compared to the CAP-MIMO system. The grating lobes also result in a loss of security and interference compared to CAP-MIMO system.

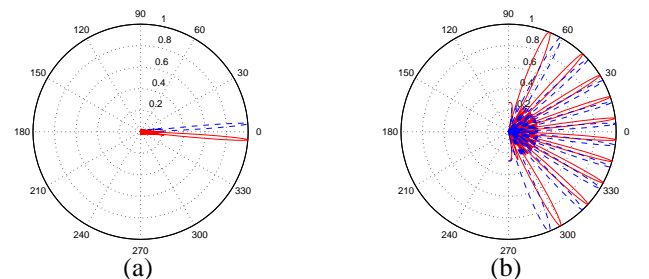


Fig. 8. CAP-MIMO versus MIMO beampatterns:  $n = 40$ ,  $p_{max} = 4$ . (a) CAP-MIMO beampatterns for two of the  $p_{max}$  beams that couple with the receiver. (b) MIMO beampatterns for the same two beams – the grating lobes associated with each beam result in loss of channel power and also lead to interference and loss of security.

## IV. IDEALIZED CAPACITY ANALYSIS: ARRAY GAIN, CHANNEL POWER, DIGITAL MODES

In this section, we outline the derivation of idealized capacity expressions in Sec. II-D. Consider a LoS with a given

<sup>2</sup>We note that  $d_{ray} \approx n_g \lambda_c/2$ .

$n$  and  $p_{max}$ . It is well-known in antenna theory that the array/beamforming gain of a linear array of aperture  $A$  is proportional to  $n = A/(\lambda_c/2)$ . This gain is achieved at the both the transmitter and receiver ends. However, for a given  $p_{max}$ , while the entire array aperture is exploited at the transmitter side for each beam, only a fraction  $1/p_{max}$  of the aperture is associated with a beam on the receiver side (see Fig. 2). As a result, the total transmit-receiver array/beamforming gain associated with each beam or digital mode is  $n^2/p_{max}$ . In the ideal setting, the transmit covariance matrix  $\mathbf{H}^H\mathbf{H}$  has  $p_{max}$  non-zero eigenvalues, each of size  $n^2/p_{max}$ , corresponding to the total channel power of  $\sigma_c^2 = n^2$ . Distributing the total transmit (SNR),  $\rho$ , equally over these  $p_{max}$  eigenmodes gives the CAP-MIMO capacity formula in (6) for  $p = p_{max}$ .

The CAP-MIMO capacity formula applies for all  $p = 1, 2, \dots, p_{max}$ . In particular, for  $p = 1$ , the CAP-MIMO capacity gives the maximum capacity for the (optimized) DISH system in which the link characteristics are adjusted so that  $p_{max} = 1$ . If  $p_{max} > 1$ , then the capacity of a DISH system which uses only a single transmission mode can be bounded as

$$\log\left(1 + \frac{\rho n^2}{p_{max}}\right) \leq C_{dish} = \log(1 + \rho \lambda_{max}) \leq \log(1 + \rho n^2) \quad (22)$$

where  $\lambda_{max}$  is the largest eigenvalue of  $\mathbf{H}^H\mathbf{H}$  and satisfies  $n^2/p_{max} = \sigma_c^2/p_{max} \leq \lambda_{max} \leq \sigma_c^2 = n^2$ . The optimized capacity of the DISH system in (5) in fact corresponds to the lower bound in (22).

The conventional MIMO system uses  $p_{max}$  antennas with spacing  $d_{ray}$  given in (1). As a result the channel power is  $p_{max}^2$  which, along with total transmit power, is equally distributed within the  $p_{max}$  eigenmodes resulting in the capacity expression (3); that is, each of the  $p_{max}$  eigenvalues of  $\mathbf{H}^H\mathbf{H}$  is of size 1 in this case.

Another way to arrive at this idealized expression for the capacity of the conventional MIMO system is that in this case the transmit array gain is  $p_{max}$  (rather than  $n$ ) and there is no receive gain (since each beam is exactly focussed on a distinct receive antenna). As a result the total transmit-receive array gain associated with each beam is  $p_{max}$  and the total transmit power associated with each mode is  $\rho/p_{max}$ . Yet another way of thinking of the power loss in the conventional MIMO system compared to CAP-MIMO is that each of the  $p_{max}$  beams in a MIMO system has  $n_g = n/p_{max}$  grating lobes and as a result on a fraction  $1/n_g$  of the maximum  $n$ -fold array/beamforming gain is achievable in the critically sampled conventional MIMO system.

## V. EXACT CAPACITY ANALYSIS

In this section, we outline exact capacity analysis of the CAP-MIMO system that refines the approximate/idealized capacity expressions in Sec. II-D for the CAP-MIMO and DISH systems. The capacity expression for the MIMO system in (3) is exact.

We consider a static point-to-point LoS channel for which the critically sampled channel matrix  $\mathbf{H}$  in (19) is deterministic

and we assume that is completely known at the transmitter and the receiver. In this case, it is well-known that the capacity-achieving input is Gaussian and is characterized by the eigenvalue decomposition of the  $n \times n$  transmit covariance matrix [16]

$$\Sigma_T = \mathbf{H}^H\mathbf{H} = \mathbf{V}\mathbf{\Lambda}\mathbf{V}^H \quad (23)$$

where  $\mathbf{V}$  is the matrix of eigenvectors and  $\mathbf{\Lambda} = \text{diag}(\lambda_1, \dots, \lambda_n)$  is the diagonal matrix of eigenvalues with  $\sum_i \lambda_i = \sigma_c^2 = n^2$ . In particular, the capacity-achieving input vector  $\mathbf{x}$  in (7) is characterized as  $\mathcal{CN}(\mathbf{0}, \mathbf{V}\mathbf{\Lambda}_s\mathbf{V}^H)$  where  $\mathbf{\Lambda}_s = \text{diag}(\rho_1, \dots, \rho_n)$  is the diagonal matrix of eigenvalues of the input covariance matrix  $E[\mathbf{x}\mathbf{x}^H]$  with  $\text{tr}(\mathbf{\Lambda}_s) = \sum_i \rho_i = \rho$ . The capacity of the critically sampled LoS link is then given by

$$\begin{aligned} C(\rho) &= \max_{\mathbf{\Lambda}_s: \text{tr}(\mathbf{\Lambda}_s) = \rho} \log |\mathbf{I} + \mathbf{\Lambda}\mathbf{\Lambda}_s| \\ &= \max_{\rho_i: \sum_i \rho_i = \rho} \sum_{i=1}^n \log(1 + \lambda_i \rho_i) \end{aligned} \quad (24)$$

As discussed earlier, out of the  $n$  possible communication modes, we expect only  $p_{max}$  modes/beams to couple to the receiver array. However, the value of  $p_{max}$  in (21) provides only an approximate baseline value for the actual channel rank for a given  $(A, R, \lambda_c)$ . In numerical results, we will replace  $p_{max}$  with the effective channel rank,  $p_{eff}$ , which we estimate as the number of dominant eigenvalues of  $\Sigma_T$  - eigenvalues that are above a certain fraction  $\gamma \in (0, 1)$  of  $\lambda_{max}$ :

$$p_{eff} = |\{i : \lambda_i \geq \gamma \lambda_{max}\}| \quad (25)$$

Using  $p_{eff}$ , the system capacity can be accurately approximated as

$$\begin{aligned} C(\rho) &\approx \max_{\rho_i: \sum_i \rho_i = \rho} \sum_{i=1}^{p_{eff}} \log(1 + \lambda_i \rho_i) \\ &\geq \sum_{i=1}^{p_{eff}} \log\left(1 + \lambda_i \frac{\rho}{p_{eff}}\right) \end{aligned} \quad (26)$$

where the last inequality corresponds to equal power allocation to all the  $p_{eff}$  modes. As we discuss in our numerical results, the effective channel rank,  $p_{eff}$ , is somewhere in the range

$$p_{eff} \in [[p_{max}], [p_{max} + 1]]. \quad (27)$$

## VI. TWO-DIMENSIONAL ARRAYS

We now outline the system model for 2D square apertures. Consider a LoS link in which both the transmitter and the receiver antennas, separated by a distance of  $R$  meters, consist of square apertures of dimension  $A \times A$   $m^2$ . The maximum number of analog and digital modes are simply the squares of the linear counterparts:

$$n_{2d} = n^2, \quad n \approx 2A/\lambda_c \quad (28)$$

$$p_{max,2d} = p_{max}^2, \quad p_{max} \approx \frac{A^2}{R\lambda_c}. \quad (29)$$

The resulting MIMO system is characterized by the  $n_{2d} \times n_{2d}$  matrix  $\mathbf{H}_{2d}$  that can be shown to be related to the 1D channel matrix  $\mathbf{H}$  in (19) via

$$\mathbf{H}_{2d} = \mathbf{H} \otimes \mathbf{H} \quad (30)$$

where  $\otimes$  denotes the kronecker product [17]. The eigenvalue decomposition of the transmit covariance matrix is similarly related to its 1D counterpart in (23)

$$\begin{aligned} \Sigma_{T,2d} &= \mathbf{H}_{2d}^H \mathbf{H}_{2d} = \mathbf{V}_{2d} \Lambda_{2d} \mathbf{V}_{2d}^H \\ \mathbf{V}_{2d} &= \mathbf{V} \otimes \mathbf{V}, \quad \Lambda_{2d} = \Lambda \otimes \Lambda. \end{aligned} \quad (31)$$

The channel power is also the square of the 1D channel power:  $\sigma_{c,2d}^2 = n_{2d}^2 = n^4 = \sigma_c^4$ . With these correspondences, the idealized capacity expressions in Sec. II and the exact capacity analysis in Sec. V can be used.

## VII. NUMERICAL RESULTS

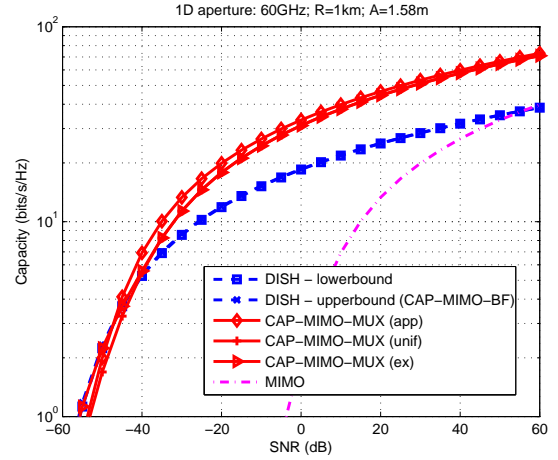
In this section, we present some representative numerical results to illustrate the capacity/SNR advantage of the CAP-MIMO system over conventional DISH and MIMO systems.

Fig. 9 compares the three systems for a long range link,  $R = 1\text{km}$ , at  $f_c = 60\text{GHz}$ . Fig. 9(a) compares linear apertures with  $A = d_{ray} = 1.58\text{m}$  corresponding to  $n = 632$  and  $p_{max} = 2$ . Fig. 9(b) presents the comparison for a corresponding 2D array with a square aperture of  $1.58 \times 1.58\text{m}^2$ , with  $n_{2d} = n^2 = 399424$  and  $p_{max,2d} = p_{max}^2 = 4$ . Two dominant eigenvalues are used in the 1D system ( $\gamma = .01$ ) and 4 in the 2D system ( $\gamma = .001$ ). In the 2D comparison, we also include the capacity of a conventional MIMO system with directional antennas that provide a 30dB gain.

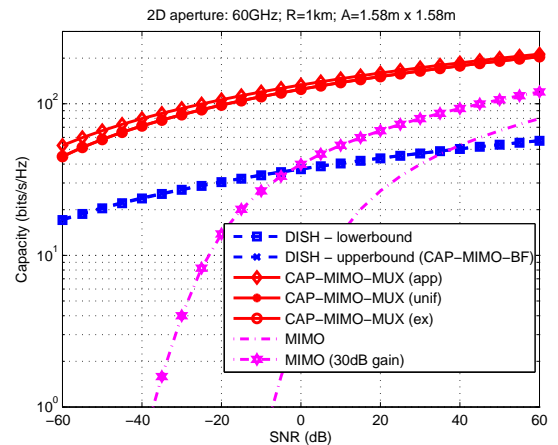
Fig. 10 compares the three systems for a short-range (indoor) link,  $R = 3\text{m}$ , at  $f_c = 80\text{GHz}$ . Fig. 10(a) compares linear apertures with  $A = d_{ray} = 7.5\text{cm}$  corresponding to  $n = 40$  and  $p_{max} = 2$ . Fig. 10(b) presents the comparison for a corresponding 2D array with a square aperture of  $7.5 \times 7.5\text{cm}^2$ , with  $n_{2d} = 1600$  and  $p_{max,2d} = 4$ . Two dominant eigenvalues are used in the 1D system ( $\gamma = .01$ ) and 4 in the 2D system ( $\gamma = .001$ ).

Interestingly, in both above examples, the condition numbers,  $\chi = \lambda_{max}/\lambda_{min}$ , for the subset of eigenvalues used in capacity calculations are  $\chi_{1d} = 14$  and  $\chi_{2d} = 216$ . Even though the channel can support up to  $p_{eff} = 2$  modes for linear arrays,  $p_{max} = 0.5$ , as calculated according to (21), emphasizing the fact that (21) is a baseline estimate (see the range for  $p_{eff}$  in (27)). The numerical results correspond to first determining  $d_{ray}$  corresponding to a given  $p_{max}$  and then calculating the array dimension as  $A = (p_{max} - 1)d_{ray}$  (rather than  $A = p_{max}d_{ray}$ ).

As evident from the above results, there is close agreement between the exact and approximate capacity estimates. Furthermore, the CAP-MIMO system exhibits very significant SNR gains over the MIMO and DISH systems at high spectral efficiencies ( $> 20$  bits/s/Hz); about 20dB for linear apertures and more than 40dB for square apertures.



(a) 1D Linear Aperture

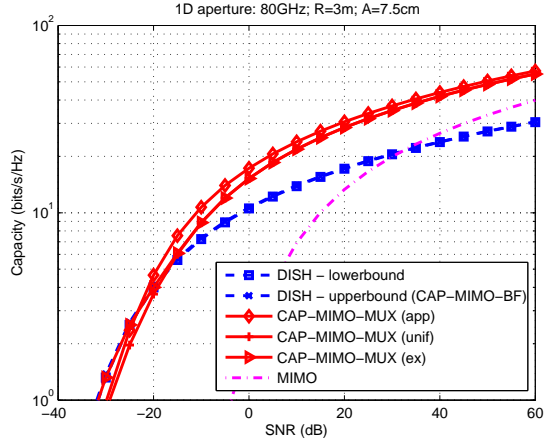


(b) 2D Square Aperture

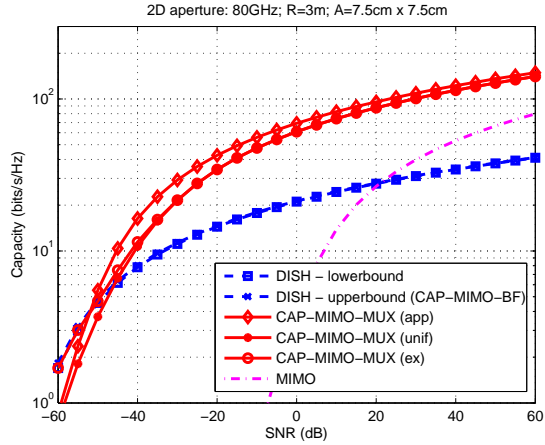
Fig. 9. Capacity versus SNR comparison between the CAP-MIMO, DISH and MIMO systems for a long-range link;  $R = 1\text{km}$ . (a) 1D linear aperture with  $A = 1.58\text{m}$ . (b) 2D square aperture.

## VIII. DETAILS OF THE CAP-MIMO TRANSCIVER

Fig. 3 shows a schematic of a DLA-based realization of a CAP-MIMO system. In this section, we provide details on the CAP-MIMO transceiver for 1D apertures. In Sec. VIII-A, we outline the simplest form for the transmitter architecture for accessing the  $p_{max}$  digital modes in a LoS link in terms of the analog transform  $\mathbf{U}_a$  and the digital transform  $\mathbf{U}_d$ . The basic architecture is based on DFTs and corresponds to directly mapping the  $p$ ,  $1 \leq p \leq p_{max}$ , digital streams into corresponding orthogonal spatial beams. In Sec. VIII-B, outline a more advanced transmitter architecture that corresponds to exact capacity analysis in Sec. V and corresponding to accessing the  $p_{max}$  digital modes in terms of  $p_{max}$  spatial eigenmodes of the LoS channel. The analog transform  $\mathbf{U}_a$ , representing the DLA, does not change but the nature of the digital transform  $\mathbf{U}_e$  is different in this case. The Fourier spatial modes, in terms of orthogonal spatial beams, in the basic architecture in Sec. VIII-A, represent approximations of the spatial eigenmodes in Sec. VIII-B. In Sec. VIII-C, we outline details of



(a) 1D Linear Aperture



(b) 2D Square Aperture

Fig. 10. Capacity versus SNR comparison between the CAP-MIMO, DISH and MIMO systems for a short-range link;  $R = 3\text{m}$ . (a) 1D linear aperture with  $A = 7.5\text{cm}$ . (b) 2D square aperture.

the corresponding DLA-based receiver architecture. In Sec. IX we discuss extensions of the CAP-MIMO system for non-identical transmit/receive antennas as well as for multipath propagation environments. Sec. X provides some additional details relating to a practical implementation of the overall CAP-MIMO system.

#### A. Basic Transmitter Architecture

The transmitter consists of two transforms. The digital transform  $\mathbf{U}_e$  maps the  $p$  independent *digital* symbols (corresponding to  $p$  simultaneous data streams) into  $n$  *analog* symbols that excite  $n$  feeds on the focal surface of the DLA. The analog transform  $\mathbf{U}_a$  represents the DLA that maps the  $n$  analog signals on the focal surface of the DLA to the spatial signals radiated by the DLA aperture. Further details on the two transforms for the simplest architecture are provided in the following subsections.

1) *The Analog Transform  $\mathbf{U}_a$* : The analog transform  $\mathbf{U}_a$  represents the analog spatial transform between the focal surface and the continuous aperture of the DLA. This continuous

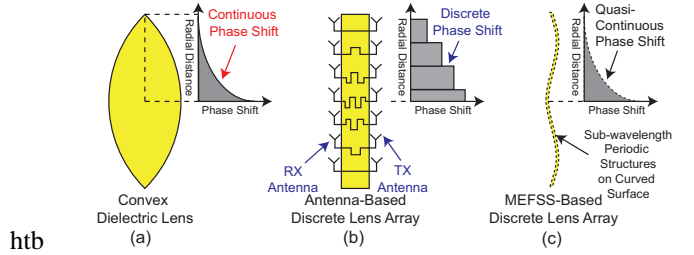


Fig. 11. Comparison between a dielectric lens (a), a traditional microwave lens composed of arrays of receiving and transmitting antennas (b), and the proposed conformal metamaterial-based microwave DLA composed of sub-wavelength periodic structures (c).

Fourier transform is affected by the wave propagation between the focal arc and the aperture of the DLA. However, consistent with the critical sampling described in Sec. III, we can accurately approximate this continuous Fourier transform by an  $n \times n$  discrete Fourier transform (DFT) matrix corresponding to critical (Nyquist) -  $\lambda_c/2$  - sampling of the aperture and the focal arc:

$$\mathbf{U}_a(\ell, m) = \frac{1}{\sqrt{n}} e^{-j \frac{2\pi \ell m}{n}}, \quad \ell \in \mathcal{I}(n), \quad m \in \mathcal{I}(n) \quad (32)$$

The index  $\ell$  represents samples on the aperture (spatial domain) and the index  $m$  represents samples on the focal arc (beamspace).

The analog component of the CAP-MIMO architecture is based on a high-resolution DLA to approximate a continuous-aperture phased-MIMO operation that enables capacity maximization of a LoS link as well beam agility for robust operation. Fig. 11 provides a comparison between a double convex dielectric lens, a conventional microwave lens composed of arrays of receiving and transmitting antennas connected through transmission lines with variables lengths [7], [8], [9], [10], [11], [12], [13], [14], and a high-resolution DLA that we plan to use in this work [15]. The high-resolution DLA is composed of a number of spatial phase shifting elements, or pixels, distributed on a flexible membrane. The local transfer function of the spatial phase shifters can be tailored to convert the electric field distribution of an incident electromagnetic (EM) wave at the lens' input aperture to a desired electric field distribution at the output aperture. These high-resolution DLAs have several unique advantages over conventional antenna-based microwave lenses, including: 1) Their spatial phase shifters are ultra-thin and their lateral dimensions can be extremely small, e.g.  $0.05\lambda_c \times 0.05\lambda_c$  as opposed to  $\lambda_c/2 \times \lambda_c/2$  in conventional DLAs [15]. This offers a greater flexibility and a higher resolution in designing the aperture phase shift profile of the lens; 2) Due to their small pixel sizes and low profiles, the high-resolution DLAs have superior performance at oblique angles of incidence with field of views of  $\pm 70^\circ$ ; and 3) Unlike conventional microwave lenses, high-resolution DLAs can operate over extremely wide bandwidths with fractional bandwidths exceeding 50%.

2) *The Digital Transform*  $\mathbf{U}_e = \mathbf{U}_d$ : The  $n \times p$  digital transform  $\mathbf{U}_e$  represents mapping of the  $p$ ,  $1 \leq p \leq p_{max}$ , independent digital signals onto the focal arc (surface in 2D), which is represented by  $n$  samples. Different values of  $p$  represent the different CAP-MIMO configurations. We denote the digital transform for the basic transmitter architecture by  $\mathbf{U}_d$ ; that is,  $\mathbf{U}_e = \mathbf{U}_d$ . For  $p = p_{max}$  (MUX configuration),  $\mathbf{U}_d$  reduces to  $p_{max} \times p_{max}$  identity transform; that is, the  $p_{max}$  inputs are directly mapped to corresponding  $p_{max}$  feeds on the focal arc. For  $p < p_{max}$ ,  $\mathbf{U}_d$  effectively maps the independent digital signals to the focal arc so that  $p$  data streams are mapped onto  $p$  beams with wider beamwidths (covering the same angular spread - subtended by the receiver array aperture). Wider beamwidths, in turn, are attained via excitation of part of the aperture. We next provide an explicit construction of  $\mathbf{U}_d$ .

For a given  $p \in \{1, 2, \dots, p_{max}\}$  representing the number of independent data streams, define the *oversampling factor* as

$$n_{os}(p) = p_{max}/p \quad , \quad p = 1, \dots, p_{max} \quad (33)$$

The  $p$  digital streams are mapped into  $p$  beams that are generated by a reduced aperture  $A(p) = A/n_{os}$  corresponding to

$$n_a(p) = n/n_{os} = np/p_{max} \quad (34)$$

(fewer) Nyquist samples. The resulting (reduced) beamspace resolution is given by

$$\Delta\theta(p) = 1/n_a(p) = (1/n)(p_{max}/p) = \Delta\theta_o n_{os}(p) \quad (35)$$

where  $\Delta\theta_o = 1/n$  is the (highest, finest) spatial resolution afforded by the full aperture. The reduced beamspace resolution corresponds to a larger beamwidth for each beam.

The  $n \times p$  digital transform  $\mathbf{U}_d$  consists of two components:  $\mathbf{U}_e = \mathbf{U}_2 \mathbf{U}_1$ . The  $n_a(p) \times p$  transform  $\mathbf{U}_1$  represents the beamspace to aperture mapping for the  $p$  digital signals corresponding to an aperture with  $n_a(p)$  (Nyquist) samples:

$$\mathbf{U}_1(\ell, m) = \frac{1}{\sqrt{n_a(p)}} e^{-j\frac{2\pi\ell m}{n_a(p)}} = \sqrt{\frac{n_{os}}{n}} e^{-j\frac{2\pi\ell m n_{os}}{n}} \quad , \quad (36)$$

where  $\ell \in \mathcal{I}(n_a(p))$ ,  $m \in \mathcal{I}(p)$ . The  $n \times n_a(p)$  mapping  $\mathbf{U}_2$  represents an oversampled - by a factor  $n/n_a(p) = n_{os}$  - IDFT (inverse DFT) of the  $n_a(p)$  dimensional (spatial domain) signal at the output of  $\mathbf{U}_1$ :

$$\mathbf{U}_2(\ell, m) = \frac{1}{\sqrt{n}} e^{j\frac{2\pi\ell m}{n}} \quad , \quad \ell \in \mathcal{I}(n) \quad , \quad m \in \mathcal{I}(n_a(p)) \quad (37)$$

For a given  $n$ ,  $p_{max}$ , and  $p$ , the  $n \times p$  composite digital transform,  $\mathbf{U}_d$ , can be expressed as

$$\begin{aligned} \mathbf{U}_d(\ell, m) &= (\mathbf{U}_2 \mathbf{U}_1)(\ell, m) = \sum_{i \in \mathcal{I}(n_a(p))} \mathbf{U}_2(\ell, i) \mathbf{U}_1(i, m) \\ &= \frac{1}{\sqrt{n_{os}}} \frac{1}{n_a} \sum_{i \in \mathcal{I}(n_a)} e^{j2\pi(\frac{\ell - m n_{os}}{n_{os}}) \frac{i}{n_a}} \\ &= \frac{1}{\sqrt{n_{os} n_a}} f_{n_a} \left( \frac{1}{n_a} \left( \frac{\ell}{n_{os}} - m \right) \right) \quad , \quad (38) \end{aligned}$$

where  $f_n(\cdot)$  is defined in (13),  $\ell \in \mathcal{I}(n)$  represent the samples of the focal arc of DLA and  $m \in \mathcal{I}(p)$  represent the indices for the digital data streams. Note that for  $p = p_{max}$  ( $n_a = n, n_{os} = 1$ ),  $\mathbf{U}_d$  reduces to a  $p_{max} \times p_{max}$  identity matrix. Even for  $p < p_{max}$ , only a subset of the outputs of  $\mathbf{U}_d$  are active, on the order of  $p_{max}$ , which can be estimated from (38).

### B. The Modified Digital Transform: Transmission on Eigenmodes

Recall the system equation (7) for the critically sampled LoS MIMO link. With reference to Fig. 3, the  $n$ -dimensional transmit signal vector  $\mathbf{x} = [x_1, \dots, x_n]^T$  is a sampled representation of the signals radiated by the DLA aperture. Furthermore,  $\mathbf{x} = \mathbf{U}_a \mathbf{x}_a$ , where (with slightly modified notation compared to Fig. 3)  $\mathbf{x}_a = [x_{a,1}, \dots, x_{a,n}]^T$  is the  $n$ -dimensional representation of the (analog) signals at the focal surface of the DLA. Finally, the  $\mathbf{x}_a = \mathbf{U}_e \mathbf{x}_e$  where  $\mathbf{x}_e = [x_{e,1}, \dots, x_{e,p}]^T$  is the  $p$ -dimensional vector of digital symbols at the input of the digital transform  $\mathbf{U}_e$ . For the basic transmitter architecture,  $\mathbf{U}_e = \mathbf{U}_d$ , where  $\mathbf{U}_d$  is defined in (38). For the basic transmitter structure, we can rewrite the system equation (7) directly in terms of  $\mathbf{x}_e$  as

$$\mathbf{r} = \mathbf{H} \mathbf{U}_a \mathbf{U}_d \mathbf{x}_e + \mathbf{w} = \mathbf{H} \mathbf{U}_{tx} \mathbf{x}_e \quad (39)$$

$$= \mathbf{H}_{red} \mathbf{x}_e \quad (40)$$

where

$$\mathbf{U}_{tx} = \mathbf{U}_a \mathbf{U}_d \quad (41)$$

is the effective  $n \times p$  transmission matrix coupling the  $p$ -dimensional vector of input digital symbols,  $\mathbf{x}_e$ , to the  $n$ -dimensional signals on the DLA aperture  $\mathbf{x} = \mathbf{U}_{tx} \mathbf{x}_e$ . It can be shown [4], [18] that the  $p$  column vectors of  $\mathbf{U}_{tx}$  form *approximate transmit (spatial) eigenmodes* of the transmit covariance matrix  $\mathbf{\Sigma}_{tx} = \mathbf{H}^H \mathbf{H}$  and transmitting over these eigenmodes is optimum (capacity-achieving) from a communication theoretic perspective. In other words,  $\mathbf{U}_{tx}$  enables optimal access to the  $p \in \{1, \dots, p_{max}\}$  digital modes in the channel. We note that for  $p < p_{max}$ , the dimension of  $\mathbf{\Sigma}_{tx}$  is reduced due to partial excitation of the transmitter DLA aperture - in other words, a reconfigured version of the LoS channel is in effect when  $\mathbf{U}_d$  is configured for transmitting  $p < p_{max}$  digital symbols simultaneously.

The approximate eigenproperty of  $\mathbf{U}_{tx} = \mathbf{U}_a \mathbf{U}_d$  gets more accurate for large  $p_{max}$ . However, for relatively small  $p_{max}$ , this approximation can be rather coarse. In this case, while  $\mathbf{U}_{tx}$  still enables access to the digital modes, the columns of  $\mathbf{U}_{tx}$  deviate from the true spatial eigenmodes. We now outline a modification of the digital transform to enable transmission onto the true spatial eigenmodes of the channel. Let  $\mathbf{\Sigma}_{tx,red} = \mathbf{H}_{red}^H \mathbf{H}_{red}$  denote the  $p \times p$  transmit covariance matrix of the reduced-dimensional  $n \times p$  channel matrix  $\mathbf{H}_{red} = \mathbf{H} \mathbf{U}_a \mathbf{U}_d$  in (40). Further, let

$$\mathbf{\Sigma}_{tx,red} = \mathbf{U}_{red} \mathbf{\Lambda}_{red} \mathbf{U}_{red}^H \quad (42)$$

denote the eigendecomposition of the  $\Sigma_{tx,red}$  where  $\mathbf{U}_{red}$  is the  $p \times p$  dimensional matrix of eigenvectors and  $\mathbf{\Lambda}_{red}$  is a  $p \times p$  diagonal matrix of (positive) eigenvalues. With the knowledge of  $\mathbf{U}_{red}$  we can modify  $\mathbf{U}_{tx}$  in (41) as

$$\mathbf{U}_{tx} = \mathbf{U}_a \mathbf{U}_d \mathbf{U}_{red} \quad (43)$$

to enable transmission onto the exact  $p$  eigenmodes for the channel where  $p \in \{1, \dots, p_{max}\}$ ,  $\mathbf{U}_d$  is the digital transform in the basic transmitter architecture defined in (38) and  $\mathbf{U}_{red}$  is defined via the eigendecomposition in (42). We note that in this case the overall  $n \times p$  digital transform  $\mathbf{U}_e$  in Fig. 3 is given by  $\mathbf{U}_e = \mathbf{U}_d \mathbf{U}_{red}$  (as opposed to  $\mathbf{U}_e = \mathbf{U}_d$  in the basic architecture).

### C. Receiver Architecture

We have mainly focussed on the transmitter architecture thus far. In this section, we outline potential receiver architectures. First of all, the receiver architecture is also DLA-based to enable efficient access to the  $p$  digital modes. That is, the receiver antenna consists of a DLA. In terms of the system equation (7), the  $n$ -dimensional received signal  $\mathbf{r}$ , representing the signal on the aperture of the receiver DLA, gets mapped to an  $n$ -dimensional signal,  $\mathbf{r}_a$ , the focal surface of the DLA via

$$\mathbf{r}_a = \mathbf{U}_a^H \mathbf{r} \quad (44)$$

where the  $n \times n$  matrix/transform  $\mathbf{U}_a^H$  represents the mapping from the receiver DLA aperture to the feeds on the focal surface. As in the case of the transmitter architecture, on the order of  $p_{max}$  elements of  $\mathbf{r}_a$  (feeds on the focal surface), out of the maximum possible  $n$ , will carry most of the significant received signal energy. A/D conversion at the receiver (including down conversion from passband to baseband) applies to these active elements of  $\mathbf{r}_a$ . Thus, the complexity of the A/D interface at the receiver has a complexity on the order of  $p_{max}$ . The resulting vector of digital symbols, derived from  $\mathbf{r}_a$  via A/D conversion, can be processed using any of a variety of algorithms known in the art (e.g., maximum likelihood detection, MMSE (minimum mean-squared-error) detection, MMSE with decision feedback) to form an estimate,  $\hat{\mathbf{x}}_e$ , at the receiver of the transmitted vector of digital symbol  $\mathbf{x}_e$ .

We note that any of a variety of space-time coding techniques may also be used at the transmitter in which digital information symbols are encoded into a *sequence/block of coded vector symbols*,  $\{\mathbf{x}_e(i)\}$ , where  $i$  denotes the time index. The receiver architecture will be modified accordingly, as known in the art. In this case, the corresponding sequence/block of received (coded) digital symbol vectors, derived from  $\mathbf{r}_a$ , is processed to extract the encoded digital information symbols.

## IX. EXTENSIONS TO DIFFERENT-SIZED ANTENNAS AND MULTIPATH CHANNELS

We have described the CAP-MIMO theory for the special case of LoS link with identical-sized antennas. We now outline the general case for LoS links and also extensions to channels with multipath propagation. We discuss the extension in the

1D case for linear apertures. Extensions to 2D apertures follow straightforwardly according to the comments in Sec. VI.

First, consider 1D LoS links in which the transmitter and receiver have antennas of different sizes,  $A_t$  and  $A_r$ , respectively. Let  $n_t \approx 2A_t/\lambda_c$  and  $n_r \approx 2A_r/\lambda_c$  denote the corresponding number of analog modes associated with the apertures as calculated in (4). The maximum number of digital modes,  $p_{max}$ , supported by the LoS link is then given by

$$p_{max} \approx \frac{A_t A_r}{R \lambda_c} \quad (45)$$

which is a generalization of (21). The details of the transceiver architecture described in Sec. VIII are then applicable, using  $n = n_t$  at the transmitter and  $n = n_r$  at the receiver.

The CAP-MIMO transceiver is also applicable to scenarios involving multipath propagation (rather than LoS propagation). Consider the general case for antennas as above corresponding to  $n_t$  and  $n_r$  analog modes at the transmitter and the receiver. An important difference in multipath channels is that the number of digital modes  $p_{max}$  is larger and depends on the *angular spreads* subtended by the multipath propagation environment at the transmitter and the receiver [4]. For simplicity, suppose that the propagation paths connecting the transmitter and receiver exhibit physical angles within the following (symmetric) ranges:

$$\phi_t \in [-\phi_{t,max}, \phi_{t,max}], \quad \phi_r \in [-\phi_{r,max}, \phi_{r,max}] \quad (46)$$

where  $\phi_t$  and  $\phi_r$  denote the physical angles associated with the propagation paths at the transmitter and receiver, respectively, and  $\phi_{t,max}$  and  $\phi_{r,max}$  denote the angular spread of the propagation environment as seen by the transmitter and receiver, respectively. In this case, as in the LoS case,  $p_{max}$  depends on the number of orthogonal spatial beams/modes on the transmitter and receiver side that lie within the angular spread of the scattering environments. To calculate  $p_{max}$ , first calculate the (normalized) angular spreads according to (10) for critical  $d = \lambda_c/2$  spacing:

$$\theta_{t,max} = 0.5 \sin(\phi_{t,max}), \quad \theta_{r,max} = 0.5 \sin(\phi_{r,max}) \quad (47)$$

The spatial resolutions (measures of beamwidths) at the transmitter and the receiver are given by

$$\Delta\theta_{o,t} = \frac{1}{n_t}, \quad \Delta\theta_{o,r} = \frac{1}{n_r}. \quad (48)$$

Then, analogous to the derivation of (21), the number of orthogonal beams at the transmitter and the receiver that couple with the multipath propagation environment are given by

$$\begin{aligned} p_{max,t} &= \frac{2\theta_{t,max}}{\Delta\theta_{o,t}} = \sin(\phi_{t,max}) n_t \approx \frac{2 \sin(\phi_{t,max}) A_t}{\lambda_c} \\ p_{max,r} &= \frac{2\theta_{r,max}}{\Delta\theta_{o,r}} = \sin(\phi_{r,max}) n_r \approx \frac{2 \sin(\phi_{r,max}) A_r}{\lambda_c} \end{aligned} \quad (49)$$

and the maximum number of digital modes supported by the multipath link is given by the minimum of the two

$$p_{max} = \min(p_{max,t}, p_{max,r}). \quad (50)$$

## X. IMPLEMENTATION DETAILS

We now provide some implementation details at the transmitter side, in particular emphasizing the D/A interface between the digital and analog transforms in Fig. 3. Similar details apply on the receiver side.

First, with a slightly different notation compared to Fig. 3, let  $\mathbf{x}_e(i) = [x_{e,1}(i), x_{e,2}(i), \dots, x_{e,p}(i)]^T$  denote the  $p$ -dimensional vector of input digital symbols at (discrete) time index  $i$ . The  $p$  input digital data streams correspond to the different components of  $\mathbf{x}_e(i)$ . The digital symbols may be from any discrete (complex) constellation  $\mathcal{Q}$  of size  $|\mathcal{Q}|$ . For example,  $|\mathcal{Q}| = 4$  for 4-QAM. Each vector symbol contains  $p \log_2 |\mathcal{Q}|$  bits of information,  $\log_2 |\mathcal{Q}|$  bits per component.

The digital transform  $\mathbf{U}_e$  is a  $n \times p$  matrix that operates on the (column) vector  $\mathbf{x}_e(i)$  for each  $i$ ; that is,

$$\mathbf{x}_a(i) = \mathbf{U}_e \mathbf{x}_e(i), \quad i = 1, 2, \dots \quad (51)$$

where  $\mathbf{x}_a(i) = [x_{a,1}(i), x_{a,2}(i), \dots, x_{a,n}(i)]^T$  is the  $n$ -dimensional vector of (digitally processed) digital symbols at the output of  $\mathbf{U}_a$  at time index  $i$ . As noted earlier, for each  $i$ , only a small subset of output symbols in  $\mathbf{x}_a(i)$ , on the order of  $p_{max}$ , is non-zero. Let this subset be denoted by  $\mathcal{O}$ . The D/A conversion and upconversion to passband occurs on this subset of symbols. The analog signal for a given component of  $\mathbf{x}_a(i)$  in  $\mathcal{O}$  can be represented as

$$x_{a,\ell}(t) = \sum_i x_{a,\ell} g(t - iT_s), \quad \ell \in \mathcal{O} \quad (52)$$

where  $x_{a,\ell}(t)$  denotes the *analog signal*, at the output of the D/A, associated with the  $\ell$ -th output data stream in the set  $\mathcal{O}$ ,  $g(t)$  denotes the analog pulse waveform associated with each digital symbol, and  $T_s$  denotes the symbol duration.

The analog signal for each active digital stream  $x_{a,\ell}(t)$  is then upconverted onto the carrier

$$x_{a,\ell}(t) \rightarrow x_{a,\ell}^C(t) \cos(2\pi f_c t) - x_{a,\ell}^S(t) \sin(2\pi f_c t), \quad \ell \in \mathcal{O} \quad (53)$$

where  $x_{a,\ell}^C(t)$  and  $x_{a,\ell}^S(t)$  denote the in-phase and quadrature-phase components of  $x_{a,\ell}(t)$ . The upconverted analog signals corresponding to the active components in  $\mathcal{O}$  are then fed to corresponding feeds on the focal arc.

Since each vector digital symbol contains  $p \log_2 |\mathcal{Q}|$  bits of information, the transmission rate in bits per second is given by

$$R = \frac{p \log_2 |\mathcal{Q}|}{T_s} \text{ bits per second} \quad (54)$$

For example, for  $p = 4$ , 4-QAM constellation, and a bandwidth of 1 GHz,  $T_s = 1$  nanosecond and the transmission rate is 8 gigabits per second.

## XI. ACKNOWLEDGEMENT

The authors would like to acknowledge the Wisconsin Alumni Research Foundation and the National Science Foundation for supporting this work.

## REFERENCES

- [1] E. Torkildson, B. Ananthasubramaniam, U. Madhow, and M. Rodwell, "Millimeter-wave MIMO: Wireless links at optical speeds," *Proc. Allerton Conference*, Sep. 2006.
- [2] C. Sheldon, M. Seo, E. Torkildson, M. Rodwell, and U. Madhow, "Four-channel spatial multiplexing over a millimeter-wave line-of-sight link," *Proc. IEEE MTT-S Int. Microwave Symp.*, June 2009.
- [3] F. Bohagen, P. Orten, and G. Oien, "Design of optimal high-rank line-of-sight MIMO channels," *IEEE Tran. Wireless Commun.*, Apr. 2007.
- [4] A. M. Sayeed, "Deconstructing multi-antenna fading channels," *IEEE Trans. Signal Processing*, vol. 50, no. 10, pp. 2563–2579, Oct. 2002.
- [5] T. Deckert and A. M. Sayeed, "A Continuous Representation of Multi-Antenna Fading Channels and Implications for Capacity Scaling and Optimum Array Design," *Proc. IEEE Globecom*, 2003.
- [6] A. M. Sayeed and V. Raghavan, "Maximizing MIMO Capacity in Sparse Multipath with Reconfigurable Antenna Arrays," *IEEE J. Select. Topics in Signal Processing (special issue on Adaptive Waveform Design for Agile Sensing and Communication)*, pp. 156–166, June 2007.
- [7] J. S. H. Schoenberg, S. C. Bundy, and Z. B. Popovic, "Two-level power combining using a lens amplifier," *IEEE Trans. Microwave Theory Techn.*, vol. 42, pp. 2480–2485, 1994.
- [8] W. Shiroma, E. Bryerton, S. Hollung, and Z. Popovic, "A quasi-optical receiver with angle diversity," in *Proceedings of the IEEE International Microwave Symposium*, San Francisco, CA, 1996, pp. 1131–1135.
- [9] D. T. McGrath, "Planar three-dimensional constrained lens," *IEEE Trans. Antennas Propagat.*, vol. 34, no. 1, p. 4650, Jan. 1986.
- [10] Z. P. S. Hollung and A. Cox, "A bi-directional quasi-optical lens amplifier," *IEEE Trans. Microwave Theory Techn.*, vol. 45, pp. 2352–2357, Dec. 1997.
- [11] Z. Popovic and A. Mortazawi, "Quasi-optical transmit/receive front end," *IEEE Trans. Microwave Theory Techn.*, vol. 48, pp. 1964–1975, Nov 1998.
- [12] A. Abbaspour-Tamijani, K. Sarabandi, and G. M. Rebeiz, "A planar filter-lens array for millimeter-wave applications," in *Proceedings of the IEEE International Antennas and Propagation*, vol. 1, Monterey, CA, June 20–26 2004, pp. 675–678.
- [13] D. M. Pozar, "Flat lens antenna concept using aperture coupled microstrip patches," *Electronics Letters*, vol. 32, no. 23, p. 21092111, Nov. 1996.
- [14] R. Sauleau and B. Bares, "Quasi axis-symmetric integrated lens antennas design rules and experimental/manufacturing trade-offs at millimeter-wave frequency," *Microwave and Optical Technology Letters*, vol. 48, no. 1, pp. 20–29, Jan. 2006.
- [15] M. A. Al-Joumayly and N. Behdad, "Design of conformal, high-resolution microwave lenses using sub wavelength periodic structures," in *2010 IEEE Antennas and Propagation Society/URSI Symposium*, Toronto, ON, July 11–17 2010.
- [16] I. E. Telatar, "Capacity of Multi-Antenna Gaussian Channels," *Eur. Trans. Telecommun.*, vol. 10, pp. 585–595, Nov. 1999.
- [17] J. W. Brewer, "Kronecker products and matrix calculus in system theory," *IEEE Trans. Circ. and Syst.*, vol. 25, no. 9, pp. 772–781, Sep. 1978.
- [18] V. Veeravalli, Y. Liang, and A. Sayeed, "Correlated MIMO wireless channels: Capacity, optimal signaling and asymptotics," *IEEE Trans. Inform. Th.*, Jun. 2005.